

Linköping University Post Print

Resonant inelastic soft-x-ray scattering from valence-band excitations in $3d^0$ compounds

S. M. Butorin, J.-H. Guo, Martin Magnuson and J. Nordgren

N.B.: When citing this work, cite the original article.

Original Publication:

S. M. Butorin, J.-H. Guo, Martin Magnuson and J. Nordgren, Resonant inelastic soft-x-ray scattering from valence-band excitations in $3d^0$ compounds, 1997, Physical Review B. Condensed Matter and Materials Physics, (55), 4242-4249.

<http://dx.doi.org/10.1103/PhysRevB.55.4242>

Copyright: American Physical Society

<http://www.aps.org/>

Postprint available at: Linköping University Electronic Press

<http://urn.kb.se/resolve?urn=urn:nbn:se:liu:diva-17474>

Resonant inelastic soft-x-ray scattering from valence-band excitations in $3d^0$ compounds

S. M. Butorin*

Department of Physics and Measurements Technology, Linköping University, S-581 83 Linköping, Sweden

J.-H. Guo, M. Magnuson, and J. Nordgren

Department of Physics, Uppsala University, Box 530, S-751 21 Uppsala, Sweden

(Received 27 September 1996)

Ti and Mn $L_{\alpha,\beta}$ x-ray fluorescence spectra of FeTiO_3 and KMnO_4 were measured with monochromatic photon excitation on selected energies across the $L_{2,3}$ absorption edges. The resulting inelastic x-ray-scattering structures and their changes with varying excitation energies are interpreted within the framework of a localized, many-body approach based on the Anderson impurity model, where the radiative process is characterized by transitions to low-energy interionic-charge-transfer excited states. Sweeping the excitation energy through the metal $2p$ threshold enhances the fluorescence transitions to the antibonding states pushed out of the band of continuous states due to strong metal $3d$ -ligand $2p$ hybridization and matching the low-photon-energy satellites in the spectra. Based on the energy position of these charge-transfer satellites with respect to the recombination peak the effective metal $3d$ -ligand $2p$ hybridization strength in the ground state of the system can be estimated directly from the experiment. [S0163-1829(97)04508-6]

I. INTRODUCTION

One of the important goals of various spectroscopies is to obtain knowledge about the electronic structure in the ground state of a system. For strongly electron-correlated systems such as $3d$ transition-metal (TM), lanthanide, and actinide compounds, the electronic structure of a system without a core hole is often described in terms of low-energy $d-d$ (or $f-f$) and charge-transfer excitations. Resonant x-ray fluorescence spectroscopy (RXFS) with monochromatic photon excitation has been shown to be a promising technique for studies of these types of excitations. Neutral $d-d$ excitations in MnO (Ref. 1) and charge-transfer (CT) excitations in cerium and uranium compounds² have been successfully studied in our earlier publications using valence-band RXFS. In this paper we discuss the application of RXFS to studies of ligand $2p \rightarrow$ metal $3d$ CT excitations in strongly covalent $3d$ TM compounds.

These CT excitations are usually described within the framework of an Anderson impurity model which provides a satisfactory description of various properties of many systems with localized states. In this model the $3d$ states of a single TM ion with the on-site Coulomb interaction U are treated as a degenerate impurity level coupled by the hybridization strength V to the ligand $2p$ band which is separated by the CT energy Δ . The interactions between neighboring impurities are neglected. It is clear then that the ground state as well as the character of the band gap in insulators can be described³ in terms of relationships between Δ , U , and V as parameters included in the model Hamiltonian. According to the $1/N$ expansion theory⁴ the effective value of V^2 is proportional to the number of $3d$ holes N ($V_{\text{eff}} \sim \sqrt{NV}$). This is the reason for strong hybridization effects in the early TM compounds where N is large in addition to large bare hybridization strength V ($3d$ wave functions are more delocalized compared to those in late TM's). In fact, V_{eff} may be large

enough to dictate the ground-state properties. While for late TM compounds the character of the band gap and its size depends on values of Δ or U , for early TM compounds the size of the gap is rather determined by the value of V_{eff} .⁵

Although the unique sets of the model parameters for different TM compounds can be established only by a consistent description of the whole variety of spectroscopic and transport properties, the spectroscopic data are often used for a preliminary estimation of the values of these parameters. Since CT effects produce so-called CT satellites in x-ray photoemission, absorption, and bremsstrahlung isochromat spectra of TM compounds, the set of the model parameters for the ground state of the system is usually derived by fitting the energy positions and intensities of CT satellites relative to the main spectral lines. However, based on first-principles calculations, it has been pointed out⁶ that the TM $3d$ -ligand $2p$ hybridization strength depends on the $3d$ occupancy and, furthermore, can be strongly affected by the presence of a core hole. As a result, V may be renormalized in a different way in different spectroscopic experiments. In this situation, those spectroscopies are particularly useful where a set of the final states of the spectroscopic process can be described by the model Hamiltonian which couples excited states with the ground state itself.

In a localized many-particle approach, the final states of the TM $3d \rightarrow 2p$ fluorescence process at the TM $2p$ threshold are the ground state (the electronic recombination peak) and low-energy excited states (the energy loss structures). The resulting resonant inelastic x-ray-scattering structures have constant energy losses with respect to the recombination peak, but exhibit a dispersionlike behavior on the emitted photon energy scale upon sweeping the excitation energy across the TM $2p$ absorption edge. Similar information can be obtained from electron-energy-loss (EELS) and optical spectroscopies. However, in contrast to all the dipole-allowed transitions in the EELS and optical-absorption data, only the TM $3d$ states as eigenvalues for the ground state

TABLE I. The site symmetry and average metal-oxygen distance (in units of Å) in studied compounds.

Compound	Symmetry	TM–O distance	Reference
FeTiO ₃	C_3	1.981	12
KMnO ₄	D_{2h}	1.629	13

Hamiltonian are probed in resonant fluorescence spectra via creation and/or annihilation of a $2p$ hole. This is especially useful in the case of multicomponent systems such as FeTiO₃ and KMnO₄, which were used in the present study as representatives of the $3d^0$ compounds.

These oxides are expected to be highly covalent systems so that their ground state can be mainly described as a mixture of $3d^0$, $3d^1\bar{L}$, and $3d^2\bar{L}^2$ configurations, where \bar{L} stands for a hole in the ligand $2p$ band. Regardless, the crystal-field interaction, the multiplet effects, and the contribution of the $3d^2\bar{L}^2$ configuration, the mechanism of the estimation of V_{eff} from resonant TM $3d \rightarrow 2p$ spectra can be demonstrated by writing a simplified ground-state Hamiltonian

$$H = \begin{pmatrix} 0 & V_{\text{eff}} \\ V_{\text{eff}} & \Delta \end{pmatrix}, \quad (1)$$

which at the same time describes the final state of RXFS. The diagonalization of this Hamiltonian gives bonding (the ground state) and antibonding states between $3d^0$ and $3d^1\bar{L}$ configurations which are separated in energy by $\sqrt{\Delta^2 + 4V_{\text{eff}}^2}$. For early TM oxides, $\Delta \ll 2V_{\text{eff}}$, and the energy separation is mainly determined by the value of V_{eff} , so that the antibonding states will appear in resonant TM $3d \rightarrow 2p$ fluorescence spectra at $\approx 2V_{\text{eff}}$ below the recombination peak. The spectral weight for transitions to these antibonding states in fluorescence spectra can be enhanced by setting the excitation energy to the TM $2p$ absorption CT satellite, which is in turn the antibonding combinations between $2p^5 3d^1$ and $2p^5 3d^2\bar{L}$ configurations.⁷ Similar resonances of antibonding states have been observed^{2,8} in the Ce $4f \rightarrow 3d$ fluorescence spectra of covalent CeO₂.

The real situation is, however, more complicated, because of the hybridization effects from the $3d^2\bar{L}^2$ configuration and because of existing transitions to nonbonding $3d^1\bar{L}$ and $3d^2\bar{L}^2$ final states.^{9–11} These transitions may have a specific resonant behavior upon sweeping the excitation energy across the TM $L_{2,3}$ ($2p \rightarrow 3d, 4s$ transitions) absorption edges, and may depend on the crystal-field symmetry which is actually different in FeTiO₃ and KMnO₄ (see Table I). In addition, for early TM compounds, the TM $2p$ spin-orbit splitting is smaller than or comparable with $2V_{\text{eff}}$, giving rise to a significant overlap of the structures of the L_3 and L_2 absorption edges⁷ and hence to a mixing of the TM $3d \rightarrow 2p_{3/2}$ and $3d \rightarrow 2p_{1/2}$ fluorescence at certain excitation energies. Furthermore, the resonant inelastic x-ray-scattering structures overlap with those of nonresonant normal fluorescence, which occurs due to direct excitations of core electrons to the continuum or due to relaxation of the system from the core-excited to core-ionized states. The difficulty in quantitatively estimating the contribution of normal fluores-

cence to the near-threshold excitation spectra complicates the analysis of the shape of resonant fluorescence.

Despite all these complications, we show that the transition to the antibonding states can be identified in the TM $L_{\alpha,\beta}$ ($3d, 4s \rightarrow 2p$ transitions) fluorescence spectra of FeTiO₃ and KMnO₄ recorded at the excitation energies set near the TM $2p$ thresholds, and that V_{eff} in the ground state of these systems can be estimated from this type of experiment.

II. EXPERIMENTAL DETAILS

The measurements were performed at the undulator beamline 7.0 of the Advanced Light Source, Lawrence Berkeley Laboratory, with a spherical grating monochromator¹⁴ using an end station described in Ref. 15. A high-resolution grazing-incidence grating spectrometer¹⁶ with a two-dimensional detector was utilized to measure x-ray fluorescence.

The FeTiO₃ (ilmenite) sample was a natural crystal obtained from the mineralogical collection of the Mineralogical Museum at the Uppsala University. The source of the crystal is Fedde, Norway. The KMnO₄ sample was a pressed pellet prepared from 97% material obtained from Aldrich Chemical Co.

The Ti and Mn $L_{\alpha,\beta}$ x-ray fluorescence spectra of FeTiO₃ and KMnO₄ were recorded with a spectrometer resolution of about 0.8 and 0.5 eV, respectively. The incidence angle of the photon beam was about 20° to the sample surface, and the spectrometer was placed in the horizontal plane at an angle of 90° with respect to the incident beam. The intensity of measured spectra were normalized to the photon flux. For energy calibration, the V $L_{1,\eta}$ ($3s \rightarrow 2p$ transitions) and Mn $L_{\alpha,\beta}$ fluorescence lines of the pure metals were used as a reference. In order to determine the excitation energies, absorption spectra at the Ti and Mn $2p$ edges were measured at the 90° incidence angle by means of total electron yield and with monochromator resolutions set to about 0.2 and 0.4 eV, respectively. The x-ray fluorescence and absorption spectra were brought to a common energy scale using the elastic peak in the fluorescence spectra recorded at the excitation energy set below the absorption edge. During x-ray fluorescence measurements, the resolution of the monochromator was about 1.5 eV for KMnO₄, and about 0.5 eV for FeTiO₃.

Upon irradiation with x rays, KMnO₄ gradually decomposes with time to compounds with lower oxidation state of manganese. This can be seen as a transformation of the $L_{2,3}$ absorption spectrum of Mn⁷⁺ into that of Mn⁴⁺. By measuring x-ray-absorption spectra in the total electron yield mode, the decomposition rate of KMnO₄ was studied and the appropriate periodicity for changing the beam position on the sample was determined. Prior to x-ray fluorescence measurements the sample surface was scraped, and then the position of the beam on the sample was changed every 3 min in order to avoid its decomposition.

Self-absorption is known to affect the shape of fluorescence spectra when there is an overlap in energy between the fluorescence and absorption spectra. Assuming a flat sample surface and regarding the geometry of our experiment, the observed intensity is given by

$$I = I_0 [1 + (\mu_{\text{out}}/\mu_{\text{in}})\tan 20^\circ]^{-1}, \quad (2)$$

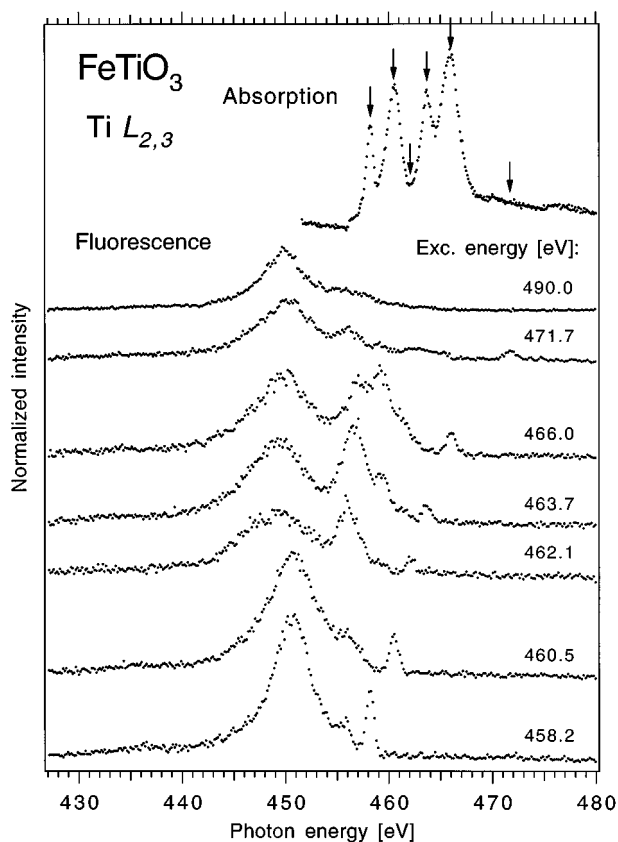


FIG. 1. The Ti $L_{2,3}$ x-ray absorption and resonant Ti $L_{\alpha,\beta}$ x-ray fluorescence spectra of FeTiO_3 . The arrows on the absorption spectrum indicate excitation energies used for fluorescence spectra.

where I_0 is the unperturbed decay intensity, and μ_{in} and μ_{out} are the absorption coefficients for the incident and outgoing radiation. We derive the values of these coefficients at the TM $2p$ threshold by normalizing the TM $L_{2,3}$ absorption spectra to known values¹⁷ below and above the corresponding absorption edges. Based on this procedure the self-absorption losses are estimated to be less than 15% for all the measured spectra.

III. RESULTS AND DISCUSSION

A. FeTiO_3

1. Resonant fluorescence

The Ti $L_{\alpha,\beta}$ x-ray fluorescence spectra of FeTiO_3 recorded at different excitation energies near the Ti $2p$ threshold are displayed in Fig. 1. The resonant part of the Ti $3d \rightarrow 2p$ fluorescence (hereafter we disregard a contribution of weak $2p-4s$ transitions in both x-ray-absorption and fluorescence spectra) exhibits dispersionlike behavior upon sweeping the excitation energy across the Ti $L_{2,3}$ absorption edges, while nonresonant normal fluorescence appears at constant energy of emitted photons. For an excitation energy of 458.2 eV, where a contribution of nonresonant normal fluorescence is expected to be small, one can see that the spectral structures extend to more than 22 eV below the recombination peak. Different structures resonate in a different way with varying excitation energies. These spectra are in contrast to what one could expect for purely tetravalent Ti (a

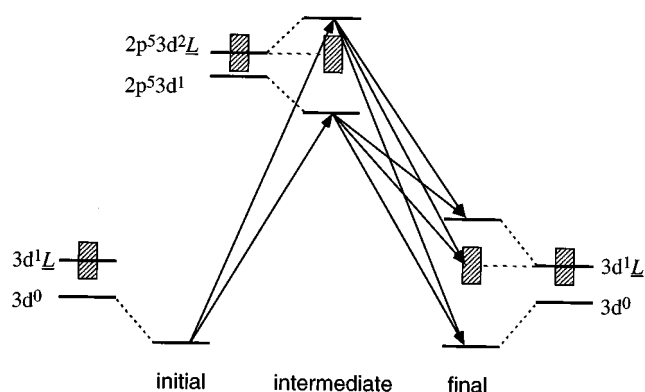


FIG. 2. A schematic representation of the resonant TM $3d \rightarrow 2p$ x-ray fluorescence process for $3d^0$ compounds. The energy levels which are labeled with electronic configurations correspond to the average multiplet energies of these configurations in the limit of $V \rightarrow 0$. The shaded rectangles represent the nonbonding states for the $3d^1L$ and $2p^53d^2L$ configurations.

single line due to the $2p^63d^0 \rightarrow 2p^53d^1 \rightarrow 2p^63d^0$ excitation-deexcitation process), thus indicating a high degree of covalency of chemical bonds and the significance of the O $2p \rightarrow$ Ti $3d$ CT in FeTiO_3 .

The resonant x-ray fluorescence process for a covalent $3d^0$ compound is shown schematically in Fig. 2, where only the two lowest electronic configurations for intermediate and final states are included for simplicity. As a result of strong TM $3d-O 2p$ hybridization in the ground and intermediate states of this process, there are radiative transitions to the final states which are the bonding (the ground state), nonbonding, and antibonding states between $3d^0$ and $3d^1L$ configurations. The nonbonding states are of the $3d^1L$ character, and are not directly coupled to the $3d^0$ state, but transitions to these states become possible through the intermediate state. The split-off antibonding state pushed out of $3d^1L$ continuous states by large V creates a low-photon-energy CT satellite in resonant fluorescence spectra.

In order to identify the spectral structures corresponding to different final states, we plotted the Ti $L_{\alpha,\beta}$ spectra of FeTiO_3 in Fig. 3 as energy-loss spectra relative to the energy of the recombination peak. Despite the overlap between the resonant x-ray inelastic scattering structures and a nonresonant normal fluorescence line which moves toward low energies upon increasing the excitation energy, some tentative assignments for the loss structures can be made. The structures appearing in the energy range between -11 and -4 eV can be attributed to the transitions to nonbonding $3d^1L$ states. The split-off antibonding satellite, schematically shown in Fig. 2, is found to be located at about -14.5 eV. The loss structures at lower energies can be assigned to transitions to nonbonding $3d^2L^2$ states.

The transition rates to different final states, and consequently, the intensities of different energy-loss features, depend on the character of the intermediate states which are represented by the Ti $L_{2,3}$ absorption spectrum. Within the ligand-field model the main four absorption peaks were ascribed to the $2p^63d^0 \rightarrow 2p^53d^1$ transitions of the Ti^{4+} ion to the states of t_{2g} (peaks at 458.2 and 463.7 eV) and e_g (460.5 and 466.0 eV) symmetry,¹⁸ regardless of some distortion of

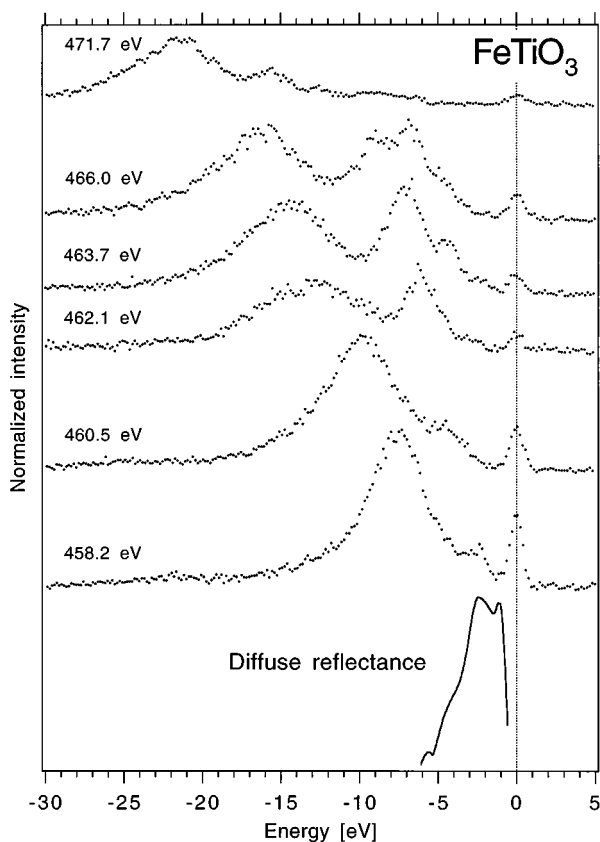


FIG. 3. The resonant Ti $L_{\alpha,\beta}$ x-ray fluorescence spectra of FeTiO_3 (dots), plotted as energy-loss spectra, relative to the energy of the recombination peak which is set at 0 eV, and the diffuse reflectance spectrum of FeTiO_3 (solid line) taken from Ref. 27.

the octahedral crystal-field symmetry in FeTiO_3 .¹² In order to describe the Ti $L_{\alpha,\beta}$ spectra of this compound, however, high covalency of the chemical bonds and CT effects should be taken into account in the description of the Ti $L_{2,3}$ absorption spectrum. Using configuration interaction cluster calculations, Okada and Kotani⁷ reproduced both the main structures and high-energy satellites in Ti $L_{2,3}$ absorption for the local O_h symmetry around the Ti ion. They assigned weak absorption satellites at about 471.5 and 477 eV to the CT satellites, which are the antibonding combinations between $2p^5 3d^1$ and $2p^5 3d^2 \underline{L}$ configurations. The large broadening of main L_2 peaks compared to those of L_3 was shown to be due to a contribution of transitions to the $2p^5 3d^2 \underline{L}$ states.

Recent measurements on CeO_2 (Refs. 2 and 8) revealed a resonant enhancement of the CT satellite (antibonding state between $4f^0$ and $4f^1 \underline{L}$ configurations) in the resonant Ce $4f \rightarrow 3d$ x-ray fluorescence spectra when the excitation energy was set to the Ce $3d$ absorption satellite (antibonding combination between $3d^9 4f^1$ and $3d^9 4f^2 \underline{L}$ configurations). Therefore, one can expect similar resonant behavior for the CT satellite in the resonant Ti $3d \rightarrow 2p$ fluorescence of FeTiO_3 . Indeed, for the excitation energy set to the Ti $L_{2,3}$ absorption satellite at 471.7 eV, there is an enhancement in the fluorescence weight at about 14.5 eV below the recombination peak, as one can see from the comparison between the 471.7 and 490.0-eV-excited Ti $L_{\alpha,\beta}$ spectra (Fig. 1). This resonance helps to determine the energy of the split-off an-

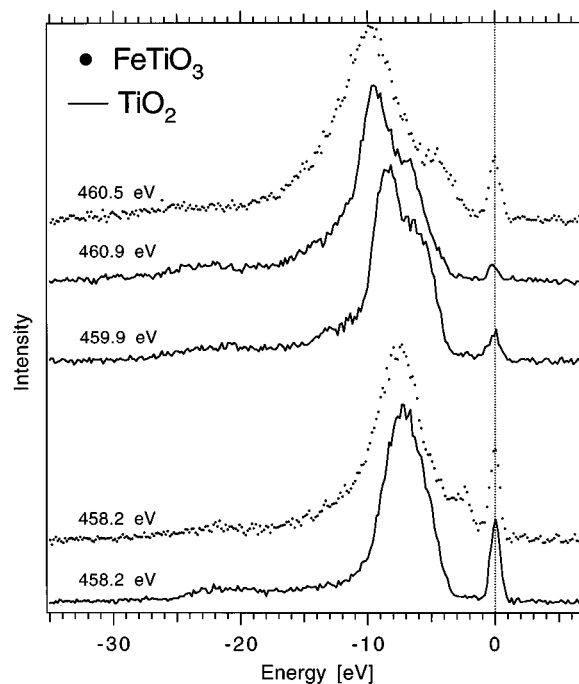


FIG. 4. The resonant Ti $L_{\alpha,\beta}$ x-ray fluorescence spectra of FeTiO_3 (dots) and TiO_2 plotted as energy-loss spectra.

tibonding state between the $3d^0$ and $3d^1 \underline{L}$ configurations (see Fig. 2), and in turn indicates the O $2p \rightarrow \text{Ti } 3d$ CT character of the absorption satellite. In light of this, the other proposed mechanisms to explain the existence of the absorption satellite such as intraligand $2p \rightarrow 3s$ excitations^{19,20} or O $2p \rightarrow \text{Ti } 4s$ shake-up²¹ appear to be less probable. The energy loss of 14.5 eV for the CT satellites in fluorescence spectra of FeTiO_3 indicates that the value of V_{eff} in the ground state of this oxide is more than 7 eV.

When the excitation energy is set to the t_{2g} and e_g peaks in the Ti L_3 edge, the most intense structures in the energy-loss spectra of FeTiO_3 (Fig. 3) appear at -7.5 and -10 eV, respectively, so that the 2.5-eV energy difference between them matches the ligand-field splitting in this compound estimated from the O $1s$ x-ray-absorption spectra.²² This suggests that the transitions to nonbonding $3d^1 \underline{L}$ final states of the resonant fluorescence process depend on the symmetry of the core-excited states, unless the observed intense structures are strongly affected by the nonresonant normal fluorescence contribution. For an excitation energy of 466.0 eV, the shape of the Ti $L_{\alpha,\beta}$ spectrum (Fig. 3) in the energy range between -11 and -4 eV resembles that of the valence band in isostructural MgTiO_3 .²³

From optical-absorption measurements the band gap in MgTiO_3 was estimated to be 3.7 eV,²⁴ while the first energy-loss structure in the resonant Ti $L_{\alpha,\beta}$ spectra of FeTiO_3 (Fig. 3) is already observed at about 2.5 eV below recombination peak. A comparison of these spectra with those of rutile TiO_2 (Ref. 25) (Fig. 4) clearly indicates the existence of additional states in the $\text{O}^{2-} \rightarrow \text{Ti}^{4+}$ CT gap of FeTiO_3 . For TiO_2 , this gap, determined as an energy difference between the recombination peak and the onset of the intense structures at low energies, is about 3.0 eV, which is in agreement with optical data for this oxide.²⁶ In order to show the origin

of the $\text{in-O}^{2-} \rightarrow \text{Ti}^{4+}$ CT-gap states in FeTiO_3 , we plotted the diffuse reflectance spectrum²⁷ of this compound in Fig. 3. The spectrum exhibits two strong optical-absorption peaks at about -1.2 and -2.4 eV, which were attributed in Ref. 27 to the $t_{2g} \rightarrow e_g$ transition of Fe^{2+} and to the $\text{Fe}^{2+} \rightarrow \text{Ti}^{4+}$ CT, respectively. The molecular-orbital calculations performed for the $(\text{FeTiO}_{10})^{14-}$ cluster²⁸ (a pair of edge-sharing octahedra containing Fe^{2+} and Ti^{4+} ions, respectively) support these assignments, thus indicating some Fe-Ti bonding. Since the $\text{Fe}^{2+} \rightarrow \text{Ti}^{4+}$ CT excitations can be as well probed in the resonant Ti $L_{\alpha,\beta}$ spectra, the structure at about 2.5 eV below the recombination peak in these spectra can, therefore, have $\text{Fe}^{2+} \rightarrow \text{Ti}^{4+}$ CT character. Alternatively, this structure may be interpreted in terms of d - d and CT excitations of Ti^{3+} as a result of possible oxygen vacancies.

2. Nonresonant normal fluorescence

The existence of nonresonant normal fluorescence at excitation energies set to the TM $2p$ absorption edge is usually considered to be due to direct core-electron excitations to the continuum or due to the Coster-Kronig process. In this case, the intermediate state is a core-ionized state for the system.

The energy for the onset of continuum states in FeTiO_3 can be determined as the energy difference between the Ti $2p$ level and the bottom of the conduction band, and can be estimated from a combination of Ti $2p$ photoemission, valence-band photoemission, and optical spectroscopies. In order to disregard a contribution of the Fe $3d$ states in the valence and conduction bands, one can use valence-band photoemission (the top of the valence band at -3.5 eV) (Ref. 29) and optical data (the band gap is 3.7 eV) (Ref. 24) for isostructural MgTiO_3 . Taking the Ti $2p_{3/2}$ binding energy in FeTiO_3 to be 459.0 eV (Ref. 30), one then finds that the onset of the continuum is at $459.0 - 3.5 + 3.7 = 459.2$ eV, i.e., about 1 eV above the t_{2g} peak in the Ti L_3 absorption edge.

The existence of the prominent 451-eV structure in the 458.2-eV-excited Ti $L_{\alpha,\beta}$ spectrum (as well as in the 460.5-eV-excited spectrum; see Fig. 1) at the emitted photon energy close to that for nonresonant normal fluorescence suggests that there might be a relaxation of the system into a core-ionized state in the intermediate state of the fluorescence process, thus resulting in normal fluorescence decay. One of the relaxation mechanisms which can occur at the excitation energies set below the onset of the continuum states was discussed by de Groot, Ruus, and Elango³¹ in the framework of CT. In particular, it has been shown that, when the $2p^5 3d^1 \rightarrow 2p^5 3d^0 \epsilon_k$ (ϵ_k corresponds to an electron in the continuum) relaxation is impossible, the $2p^5 3d^2 L \rightarrow 2p^5 3d^1 L \epsilon_k$ channel can be energetically allowed. Considering a significant admixture of the $3d^1 L$ configuration in the ground state of the system (the $3d^1 L$ contribution was estimated to be about 48% from the analysis of different high-energy spectroscopic data⁵), the assumption about the relaxation origin of the 451-eV structure in the 458.2-eV-excited Ti $L_{\alpha,\beta}$ spectrum would be reasonable. However, we believe that this structure is to a large extent due to resonant fluorescence. The main argument that this is not a relaxation is the shape of the fluorescence spectrum (Fig. 1) recorded at the excitation energy of 462.5 eV (in a dip between L_3 and L_2 absorption lines). The spectrum exhibits a similar intense structure at about 7 eV below the recombination peak, while

the excitation energy is set below the $2p_{1/2} \rightarrow 3d$ multiplet¹⁸ and, hence, no L_β normal fluorescence can be observed as a result of the relaxation process mentioned above. Furthermore, this structure can hardly be attributed to so-called Raman scattering below the Ti L_2 absorption edge, because such Raman-scattering spectra are usually quite broad. On the other hand, $2p^5 3d^2 L$ states have been shown⁷ to contribute to the region between the e_g line of L_3 and the t_{2g} line of L_2 so that the high-energy part of the 462.5-eV-excited Ti $L_{\alpha,\beta}$ spectrum most likely belongs to resonant fluorescence as a result of the decay of these states.

At an excitation energy of 490.0 eV, nonresonant normal fluorescence dominates in Ti $L_{\alpha,\beta}$ spectra of FeTiO_3 . The main maximum at about 450.5 eV can be assigned mainly to $2p^5 3d^1 L \rightarrow 2p^6 3d^0 L$ transitions. The energies of the most intense transitions can be estimated from simple energetical considerations. The strongest peak of Ti $2p$ photoemission which has mainly $2p^5 3d^1 L$ character^{7,9} is located at 459.0 eV.³⁰ Assuming the binding energy of the $3d^0 L$ maximum to be about 8 eV, which is similar to what was found for TiO_2 from resonant valence-band photoemission data,^{10,32} we obtain $459.0 - 8.0 = 451.0$ eV as the emission energy for the intense $2p^5 3d^1 L \rightarrow 2p^6 3d^0 L$ transitions. In addition, it has been shown^{7,9} that the Ti $2p$ photoemission spectrum contains a significant amount of $2p^5 3d^2 L^2$ component, which may in principle decay radiatively. Therefore, one can expect some contribution of $2p^5 3d^2 L^2 \rightarrow 2p^6 3d^1 L^2$ transitions to the normal fluorescence spectrum.

The normal fluorescence structures also originate from so-called shake-up, shake-off, and $2p_{1/2} 2p_{3/2} 3d$ Coster-Kronig processes. At high excitation energies a contribution of these processes to normal fluorescence is mainly determined by the admixture of the $3d^2 L^2$ configuration in the ground state of the system, giving rise to $2p^5 3d^1 L^2 \rightarrow 2p^6 3d^0 L^2$ transitions. At excitation energies set to the $2p_{1/2}$ threshold, the $2p_{1/2} 2p_{3/2} 3d$ Coster-Kronig process also leads to $2p^5 3d^1 L \rightarrow 2p^6 3d^0 L$ and $2p^5 3d^2 L^2 \rightarrow 2p^6 3d^1 L^2$ transitions due to the $3d^1 L$ and $3d^2 L^2$ components in the ground state. An enhancement of normal L_α fluorescence due to this Coster-Kronig decay upon sweeping the excitation energy across the L_2 edge is, however, not significant, as one can see in Fig. 1.

B. KMnO_4

1. Resonant fluorescence

For KMnO_4 , the Mn $2p$ spin-orbit splitting is comparable with $2V_{\text{eff}}$. Therefore, it is difficult to identify charge-transfer satellites in the Mn L_3 absorption edge^{33,34} because of the overlap of these satellites with Mn L_2 structures. In this case, the sensitivity of the radiative decay and the shape of resonant Mn $L_{\alpha,\beta}$ spectra to the character of core-excited, intermediate states is especially useful. These Mn $L_{\alpha,\beta}$ spectra of KMnO_4 recorded at various excitation energies across the Mn $2p$ threshold are displayed in Fig. 5. At excitation energies set to the Mn L_3 edge (640.5 and 644.9 eV) an overall shape of the Mn L_α spectra, consisting of the recombination peak, prominent structure a few eV below it, and low-energy tail is similar to that of resonant Ti L_α spectra of FeTiO_3 , despite differences in the crystal structure of these compounds.^{12,13} For the tetrahedral symmetry of the crystal

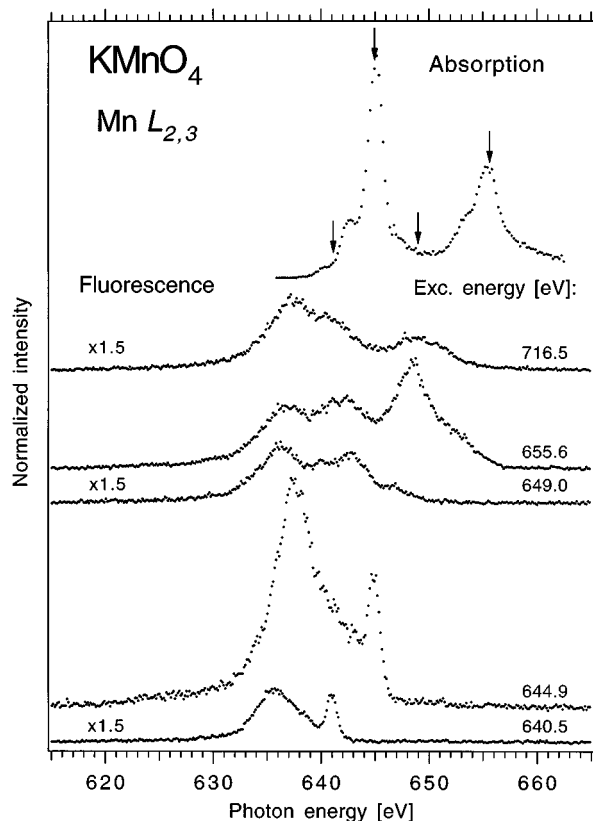


FIG. 5. The Mn $L_{2,3}$ x-ray absorption and resonant Mn $L_{\alpha,\beta}$ x-ray fluorescence spectra of KMnO_4 . The arrows on the absorption spectrum indicate excitation energies used for fluorescence spectra.

field the e_g -derived states of the $2p^53d^1$ multiplet split toward low energies, so that the main Mn L_3 and L_2 absorption peaks in KMnO_4 have mostly t_{2g} -like character.³³ As in the case of FeTiO_3 , the shape of resonant Mn $L_{\alpha,\beta}$ spectra of KMnO_4 indicates a strong covalency of the Mn-O chemical bonds in the latter compound.

In order to see similarities and differences between optical absorption, electron-energy-loss, and resonant Mn $L_{\alpha,\beta}$ spectra of KMnO_4 , we placed all of them on the same energy scale in Fig. 6. The shape of the resonant part of the Mn L_α fluorescence within 10 eV below the recombination peak is somewhat similar to that of optical absorption, although fine structures in x-ray fluorescence spectra are smeared out due to a significant spread of the excitation energy and due to experimental broadening from the spectrometer. It is known that the shape of resonant fluorescence spectra is sensitive to the width of the excitation energy.³⁷ For KMnO_4 , this width (1.5 eV) in x-ray fluorescence measurements was three times larger than that (0.5 eV) for FeTiO_3 . As a result, the insulating gap of KMnO_4 , which was estimated to be only about 1.6 eV based on transport³⁸ and EELS (Refs. 35 and 39) data is completely smeared out in resonant Mn $L_{\alpha,\beta}$ spectra in Fig. 6.

Referring to the discussion for FeTiO_3 , the spectral weight of resonant Mn $L_{\alpha,\beta}$ fluorescence of KMnO_4 within ~ 10 eV below the recombination peak can be associated with transitions to nonbonding $3d^1\bar{L}$ states. The difference in energy of the prominent structures at 5.5–7 eV below the recombination peak between the 640.5- and 644.9-eV-

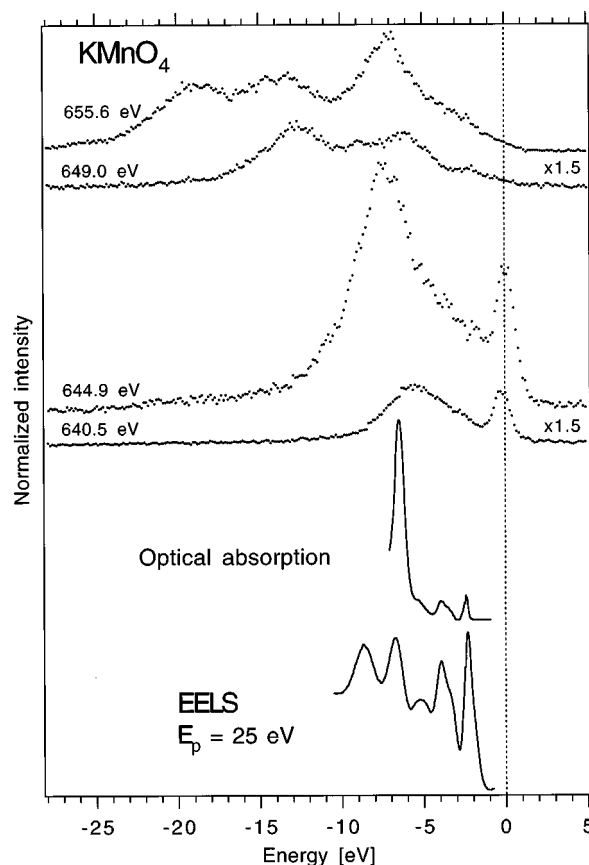


FIG. 6. The resonant Mn $L_{\alpha,\beta}$ x-ray fluorescence spectra of KMnO_4 plotted as energy-loss spectra, relative to the energy of the recombination peak which is set at 0 eV, and the electron-energy-loss spectrum of KMnO_4 (Ref. 35) recorded at the primary electron energy of 25 eV. The optical-absorption spectrum of an aqueous solution of KMnO_4 is taken from Ref. 36.

excited fluorescence spectra and between the 649.0- and 655.6-eV-excited spectra is similar to the value of the ligand-field splitting (~ 1.5 eV) in KMnO_4 , as determined from O $1s$ x-ray-absorption spectra.^{33,34}

We find the CT satellite (an antibonding combination between $3d^0$ and $3d^1\bar{L}$ configurations) in resonant x-ray scattering of KMnO_4 (Fig. 6) to be located at about -13 eV, based on resonances which are observed at this energy in the 649.0- and 655.6-eV-excited spectra. Although, for the former spectrum, this resonance appears at an energy close to that of normal fluorescence (see also Fig. 5), it cannot entirely originate from the normal fluorescence transitions. The contribution of these transitions to the 649.0-eV-excited spectrum is expected to be small based on the analysis of the nonradiative decay for the same excitation energy. The normal Auger line, a counterpart of the normal fluorescence decay, is fairly weak in the corresponding resonant photoemission spectrum of KMnO_4 .³⁴

The enhancement of the spectral weight at about -13 eV in the 655.6-eV-excited Mn $L_{\alpha,\beta}$ spectrum of KMnO_4 (Fig. 6) cannot be caused by the $2p_{1/2}2p_{3/2}3d$ Coster-Kronig process, which becomes possible at excitation energies set to the L_2 edge. As for FeTiO_3 this process can give rise only to $2p^53d^1\bar{L} \rightarrow 2p^63d^0\bar{L}$ and $2p^53d^2\bar{L}^2 \rightarrow 2p^63d^1\bar{L}^2$ transitions and, thus, is expected to enhance the nonresonantlike,

normal L_{α} line. Since the $3d^1\bar{L}^1$ configuration is likely to be dominant in the ground state of KMnO_4 , the $2p_{1/2}2p_{3/2}3d$ Coster-Kronig decay with excitation at the Mn $2p_{1/2}$ threshold should lead to a spectral weight enhancement in the photon-energy range of the main nonresonantlike L_{α} peak (~ 637.6 eV on the photon-energy scale) which corresponds mainly to $2p^53d^1\bar{L}^1 \rightarrow 2p^63d^0\bar{L}^1$ transitions (see below). A further argument against the Coster-Kronig origin of the structure at -13 eV in the 655.6 -eV-excited Mn $L_{\alpha,\beta}$ spectrum (Fig. 6) comes from the analysis of the shape of this spectrum between -10 and 0 eV. If the $2p^53d^2\bar{L}$ and $2p^53d^3\bar{L}^2$ components of the intermediate state decayed mostly through the Coster-Kronig process then the intensity of the $3d^1\bar{L}$ structure at -7 eV would be strongly suppressed with respect to that of the recombination peak. The corresponding Mn $L_{\alpha,\beta}$ spectrum, however, shows the opposite behavior: the $3d^1\bar{L}$ structure is intense, and the recombination peak is weak. Thus, taking into account the arguments discussed above, the resonances -13 eV in the 649.0 -eV- and 655.6 -eV-excited spectra (Fig. 6) can be regarded as a manifestation of the CT satellite, which is an antibonding combination between $3d^0$ and $3d^1\bar{L}$ configurations.

For KMnO_4 , this satellite, as well as the one corresponding to transitions to the nonbonding $3d^2\bar{L}^2$ states, have smaller energy losses with respect to the recombination peak than those for FeTiO_3 (13 eV versus 14.5 eV for the former satellite, and 18 eV versus 22 eV for the latter one). The observed energy differences can be tentatively explained by a difference in the value of Δ between these compounds. Δ is expected to be smaller in KMnO_4 due to the higher oxidation state for TM and, hence, higher covalency of TM-O chemical bonds than those in FeTiO_3 . For oxides of tetravalent Ti such as TiO_2 and SrTiO_3 , the values of Δ and U , estimated from the analysis of various high-energy spectroscopic data^{5,10} are 4.0 and 4.5 eV, respectively. Assuming U to be the same in KMnO_4 and taking $V_{\text{eff}} = 7.0$ eV, one can roughly estimate the value of Δ in this compound by diagonalizing a simplified Hamiltonian so that its eigenvalues match the energies of the resonant fluorescence structures associated with transitions to both nonbonding and antibonding states between different electronic configurations with respect to the recombination peak. This gives about 2 eV for the value of Δ in KMnO_4 .

2. Nonresonant normal fluorescence

In KMnO_4 the chemical potential is located close to the bottom of the conduction band.³⁵ Therefore, the onset of the continuum states in the Mn $2p$ absorption spectrum of this compound can be expected to be at about 645.5 eV based on the same value for the Mn $2p_{3/2}$ binding energy as determined from core-level x-ray-photoemission spectroscopy.³⁴ Indeed, the appearance of the normal Auger line, corresponding to the decay from the core-ionized state, was detected in resonant photoemission spectra of KMnO_4 only at excitation energies higher than 645.5 eV.³⁴ Accurate quantitative estimations of the contribution of normal fluorescence into Mn $L_{\alpha,\beta}$ spectra excited at different excitation energies near the

Mn $2p$ threshold are, however, hampered due to an overlap of structures belonging to normal fluorescence with resonant inelastic x-ray-scattering structures.

For an excitation energy of 716.5 eV, normal fluorescence dominates in the Mn $L_{\alpha,\beta}$ spectrum of KMnO_4 . The spectrum is similar to those obtained earlier^{40,41} on samples cooled with liquid nitrogen using x-ray tubes as a source of the radiation. Expecting the main Mn $2p_{3/2}$ photoemission line to have largely $2p^53d^1\bar{L}$ character, and based on the energy difference between this peak (~ 645.5 eV) and the $3d^0\bar{L}$ maximum (~ 7.5 eV) in resonant Mn $3d$ photoemission,³⁶ one can assign the main peak (~ 647.6 eV) in the normal Mn L_{α} fluorescence spectra to $2p^53d^1\bar{L}^1 \rightarrow 2p^63d^0\bar{L}^1$ transitions. This peak is accompanied by a high-energy shoulder which is more pronounced than that in the normal fluorescence spectra of FeTiO_3 . Since the $3d^2\bar{L}^2$ and $2p^53d^2\bar{L}^2$ admixtures in the ground and intermediate states of the fluorescence process should be larger in KMnO_4 compared to those in FeTiO_3 , this may be the reason for the increase in the intensity of the shoulder as a result, for example, of $2p^53d^2\bar{L}^2 \rightarrow 2p^63d^1\bar{L}^2$ transitions.

IV. CONCLUSIONS

To summarize, the TM $L_{\alpha,\beta}$ x-ray fluorescence spectra of FeTiO_3 and KMnO_4 recorded at excitation energies set in the vicinity of the TM $2p$ threshold exhibit features which suggest the validity of the localized, many-body description of the resonant TM $3d \rightarrow 2p$ fluorescence process in these compounds. In particular, specific spectral changes with varying excitation energies can be explained based on the Anderson impurity model, so that resulting inelastic x-ray-scattering spectra are associated with transitions to the low-energy interionic CT-excited states. The corresponding analysis of these spectra gives the estimates for the value of TM $3d$ -O $2p$ hybridization strength used in a set of model parameters to describe the ground state of the studied systems.

At the same time, the existence of the large spectral weight in all the recorded fluorescence spectra at the photon energies close to that of normal $L_{\alpha,\beta}$ fluorescence may be an indication of partial relaxation to the core-ionized state in the intermediate state of the resonant fluorescence process as a result of a significant degree of the $3d$ delocalization in the $3d^0$ compounds.

ACKNOWLEDGMENTS

We would like to thank Dr. P. Nysten for providing the FeTiO_3 crystal. S.M.B. acknowledges fellowship support from the NFR (the Swedish Natural Science Research Council). This work was supported by NFR and Göran Gustafsson Foundation for Research in Natural Sciences and Medicine. The experiments at ALS were also supported by the director, Office of Energy Research, Office of Basic Energy Science, Material Science Division of the U.S. Department of Energy, under Contract No. DE-AC03-76SF00098.

- *Also at MAX-lab, University of Lund, Box 118, S-221 00 Lund, Sweden. On leave from the Institute of Metal Physics, Ekaterinburg, Russia.
- ¹S. M. Butorin, J.-H. Guo, M. Magnuson, P. Kuiper, and J. Nordgren, *Phys. Rev. B* **54**, 4405 (1996).
- ²S. M. Butorin, D. C. Mancini, J.-H. Guo, N. Wassdahl, J. Nordgren, M. Nakazawa, S. Tanaka, T. Uozumi, A. Kotani, Y. Ma, K. E. Myano, B. A. Karlin, and D. K. Shuh, *Phys. Rev. Lett.* **77**, 574 (1996).
- ³J. Zaanen, G. A. Sawatzky, and J. W. Allen, *Phys. Rev. Lett.* **55**, 418 (1985).
- ⁴O. Gunnarsson and K. Schönhammer, *Phys. Rev. B* **28**, 4315 (1983).
- ⁵A. Kotani, T. Uozumi, K. Okada, and J. C. Parlebas, in *Spectroscopy of Mott Insulators and Correlated Metals*, edited A. Fujimori and Y. Tokura (Springer-Verlag, Berlin, 1995), p. 139.
- ⁶O. Gunnarsson, O. K. Andersen, O. Jepsen, and J. Zaanen, *Phys. Rev. B* **39**, 1708 (1989); O. Gunnarsson and K. Schönhammer, *ibid.* **40**, 4160 (1989).
- ⁷K. Okada and A. Kotani, *J. Electron. Spectrosc.* **71**, R1 (1995).
- ⁸M. Nakazawa, S. Tanaka, T. Uozumi, and A. Kotani, *J. Electron. Spectrosc.* **79**, 183 (1996).
- ⁹K. Okada, T. Uozumi, and A. Kotani, *J. Phys. Soc. Jpn.* **63**, 3176 (1994).
- ¹⁰T. Jo and A. Tanaka, *J. Phys. Soc. Jpn.* **64**, 676 (1995).
- ¹¹T. Uozumi, K. Okada, A. Kotani, Y. Tezuka, and S. Shin, *J. Phys. Soc. Jpn.* **65**, 1150 (1996).
- ¹²B. A. Wechsler and C. T. Prewitt, *Am. Min.* **69**, 176 (1984).
- ¹³G. J. Palenik, *Inorg. Chem.* **6**, 503 (1967).
- ¹⁴H. A. Padmore and T. Warwick, *J. Synchrotron Radiat.* **1**, 27 (1994), and references therein.
- ¹⁵J.-H. Guo, N. Wassdahl, P. Skytt, S. M. Butorin, L.-C. Duda, C. J. Englund, and J. Nordgren, *Rev. Sci. Instrum.* **66**, 1561 (1995).
- ¹⁶J. Nordgren, G. Bray, S. Cramm, R. Nyholm, J.-E. Rubensson, and N. Wassdahl, *Rev. Sci. Instrum.* **60**, 1690 (1989).
- ¹⁷B. L. Henke, E. M. Gullikson, and J. C. Davis, *At. Data Nucl. Data Tables* **54**, 181 (1993).
- ¹⁸F. M. F. de Groot, J. C. Fuggle, B. T. Thole, and G. A. Sawatzky, *Phys. Rev. B* **41**, 928 (1990).
- ¹⁹D. K. G. de Boer, C. Haas, and G. A. Sawatzky, *Phys. Rev. B* **29**, 4401 (1984).
- ²⁰G. van der Laan, *Phys. Rev. B* **41**, 12 366 (1990).
- ²¹M. Ohno and P. Decleva, *Phys. Rev. B* **49**, 818 (1994).
- ²²R. Brydson, H. Sauer, W. Engel, and F. Hofer, *J. Phys.* **4**, 3429 (1992).
- ²³T. N. Bondarenko, Yu. A. Teterin, and A. S. Baev, *Dokl. Akad. Nauk SSSR Khim.* **279**, 109 (1984) [*Dokl. Chem. Proc. Acad. Sci. USSR* **279**, 381 (1984)].
- ²⁴L. G. J. de Haart, A. J. de Vries, and G. Blasse, *Mater. Res. Bull.* **19**, 817 (1984).
- ²⁵S. M. Butorin, J.-H. Guo, M. Magnuson, and J. Nordgren (unpublished).
- ²⁶D. C. Gronemeyer, *Phys. Rev.* **87**, 876 (1952).
- ²⁷R. G. J. Strens and B. J. Wood, *Mineral. Mag.* **43**, 347 (1979).
- ²⁸D. M. Sherman, *Phys. Chem. Miner.* **14**, 364 (1987).
- ²⁹This value is derived by adjusting the energy scale, common for the set of valence-band photoemission spectra reported in Ref. 23, so that this scale for TiO₂, SrTiO₃, and BaTiO₃ is in agreement with what was measured for these compounds by different research groups [see, for example, K. W. Goodman and V. E. Henrich, *Phys. Rev. B* **50**, 10 450 (1994); Y. Tezuka, S. Shin, T. Ishii, T. Ejima, S. Suzuki, and S. Sato, *J. Phys. Soc. Jpn.* **63**, 347 (1994); A. Fujimori, I. Hase, Y. Tokura, M. Abbate, F. M. F. de Groot, J. C. Fuggle, H. Eisaki, and S. Uchida, *Physica B* **186-188**, 981 (1993); S. W. Robey, L. T. Hudson, C. Eylem, and B. Eichorn, *Phys. Rev. B* **48**, 562 (1993)]. The derived value is also consistent with the expectation that in MgTiO₃ the chemical potential should be near the bottom of the conduction band as in other tetravalent Ti compounds.
- ³⁰P. D. Schulze, T. E. Neil, S. L. Shaffer, R. W. Smith, and D. S. McKay, *J. Vac. Sci. Technol. A* **3**, 6 (1985).
- ³¹F. M. F. de Groot, R. Ruus, and M. Elango, *Phys. Rev. B* **51**, 14 062 (1995).
- ³²Y. Tezuka, S. Shin, and T. Ishii, Technical Report of ISSP, Ser. A, No. 2943, February 1995.
- ³³R. Brydson, L. A. J. Garvie, A. J. Graven, H. Sauer, F. Hofer, and G. Gresse, *J. Phys.* **5**, 9379 (1993).
- ³⁴F. Reinert, P. Steiner, R. Zimmermann, R. Claessen, and S. Hüfner, *Z. Phys. B* **99**, 229 (1996).
- ³⁵F. Reinert, S. Kumar, P. Steiner, R. Claessen, and S. Hüfner, *Z. Phys. B* **94**, 431 (1994).
- ³⁶P. Mullen, K. Schwochau, and C. K. Jørgensen, *Chem. Phys. Lett.* **3**, 49 (1969).
- ³⁷See, for example, Y. Luo, H. Ågren, F. Gel'mukhanov, J. Guo, P. Skytt, N. Wassdahl, and J. Nordgren, *Phys. Rev. B* **52**, 14 479 (1995).
- ³⁸A. M. Trubitsyn, A. A. Kabanov, V. V. Boldyrev, and A. K. Makhovik, *Sov. Phys. Dokl.* **6**, 972 (1964).
- ³⁹F. Reinert, P. Steiner, Th. Engel, and S. Hüfner, *Z. Phys. B* **99**, 223 (1996).
- ⁴⁰A. P. Sadovskii, E. A. Kravtsova, and L. N. Mazalov, *Izv. Sibir. Otd. Akad. Nauk USSR, Ser. Khim.* **4**, 62 (1975).
- ⁴¹K. H. Hallmeier, R. Szargan, K. Fritsche, and A. Meisel, *Phys. Scr.* **35**, 827 (1987).